Sensors and Actuators B 182 (2013) 95–103

Contents lists available at SciVerse ScienceDirect

Sensors and Actuators B: Chemical

journal homepage: www.elsevier.com/locate/snb

Interface reaction and its effect on the performance of a CO_2 gas sensor based on $Li_{0.35}La_{0.55}TiO_3$ electrolyte and Li_2CO_3 sensing electrode

Junro Yoon[a,b], Gary Hunter[c], Sheikh Akbar[a,b,*], Prabir K. Dutta[a,d,*]

[a] Center for Industrial Sensors and Measurements, The Ohio State University, 2041 College Road, Columbus, OH 43210, United States
[b] Department of Materials Science and Engineering, The Ohio State University, 2041 College Road, Columbus, OH 43210, United States
[c] NASA Glenn Research Center, Cleveland, OH, United States
[d] Department of Chemistry, The Ohio State University, 100W 18th Avenue, Columbus, OH 43210, United States

ARTICLE INFO

Article history:
Received 4 September 2012
Received in revised form 12 February 2013
Accepted 27 February 2013
Available online 6 March 2013

Keywords:
CO_2 sensor
Electrochemical device
Lithium lanthanum titanate
Electrode–electrolyte interface
Interface reaction
Lithium ion conductor

ABSTRACT

A new potentiometric CO_2 gas sensor using lithium–lanthanum–titanate ($Li_{0.35}La_{0.55}TiO_3$, LLTO) electrolyte, Li_2CO_3 sensing electrode, and $Li_2TiO_3 + TiO_2$ reference electrode was investigated. The microstructure and electrical properties of the optimized solid electrolyte were examined and the measured conductivity values were found consistent with those reported in literature. The performance of the sensor depended both on the fabrication temperature and the sensor operation temperature. Sensors with the sensing electrode fabricated above 500 °C performed poorly. For sensing electrodes fabricated at 500 °C, as the sensing temperature increased from 300 to 450 °C, the performance of the sensor improved (near Nernstian response), but above 450 °C, the sensor degraded. The proposed hypothesis for the degradation beyond 450 °C is that at low levels of CO_2 (ppb in the background), Li_2CO_3 reacts with LLTO resulting in insertion of Li^+ into LLTO that causes changes in the electrical properties of the electrolyte. Poor performance of sensors fabricated at 700 °C was due to formation of a new phase, $LaLi_{1/3}Ti_{2/3}O_3$. Thermodynamic calculations combined with X-ray diffraction of the reaction products are used to support the hypothesis. Introduction of high concentrations of CO_2 (~99.99%) during sensor fabrication (650 °C) eliminated the reaction between Li_2CO_3 and LLTO, and also facilitated the bonding between the electrode and the electrolyte. As for long-term device performance, it is shown that the sensor can measure changes in CO_2 concentrations reproducibly below temperatures of 450 °C, as long as it is operated in conditions where there is a background of CO_2, such as in ambient atmosphere or combustion environments. The sensor exhibits minimal interference toward oxygen, but significant interference to humidity.

1. Introduction

Environmental monitoring of greenhouse gases [1,2], health care [3], in-door air quality control, fire detection systems [4,5], and many industries [6] require carbon dioxide (CO_2) sensors. Various types of CO_2 sensors have been developed, and among these, electrochemical and optical sensors have been the most studied. Electrochemical sensors can exhibit higher sensitivity, selectivity, can be readily miniaturized and often cost less [7–10].

Extensive research on electrochemical CO_2 sensors has been conducted based on sodium ion conductors such as Na^+-β/β''-alumina, Na_2O-Al_2O_3-$4SiO_2$, and NASICON ($Na_3Zr_2Si_2PO_{12}$) [9,11,12]. Sensors based on sodium ion conductors often exhibit drift under dry and/or humid atmosphere [13–15], and is caused by multiple reasons such as instability of the electrolyte; reaction with metal-carbonate and additional phase formation at the electrode–electrolyte interface [16–20]. As an alternative, less humidity-dependent lithium ion conductors have drawn attention. Sensors based on lithium ion conductors have been reported [21–30].

Our previous studies focused on electrochemical CO_2 sensors with Li_3PO_4 electrolyte, alkali metal carbonate sensing electrode, and a bi-phase mixture of Li_2TiO_3 and TiO_2 reference electrode [27,31]. Li_3PO_4 has poor ionic conductivity at lower temperatures (even at 500 °C the conductivity is 5.58×10^{-6} S/cm). Thus, there is interest in exploring alternate lithium ion conductors that have higher conductivity at low temperatures [32].

Lithium–lanthanum–titanate ($Li_{3x}La_{((2/3)-x)}\square_{((1/3)-2x)}TiO_3$, $0 < x < 0.16$, LLTO) is reported to have high ionic conductivity at

* Corresponding authors at: Center for Industrial Sensors and Measurements, The Ohio State University, 2041 College Road, Columbus, OH 43210, United States. Tel.: +1 6142924532.
E-mail addresses: akbar@matsceng.ohio-state.edu (S. Akbar), dutta.1@osu.edu, dutta@chemistry.ohio-state.edu (P.K. Dutta).

0925-4005/$ – see front matter © 2013 Elsevier B.V. All rights reserved.
http://dx.doi.org/10.1016/j.snb.2013.02.104

room temperature ($\sigma_{grain} = 1 \times 10^{-3}$ S/cm, $\sigma_{grain\ boundary} = 7.5 \times 10^{-5}$ S/cm, and $\sigma_{total} = 7.5 \times 10^{-5}$ S/cm at 25 °C when $x \approx 0.11$) [33,34]. Materials based on LLTO has been investigated as a pH sensor [35], an electrolysis separator [36], and lithium battery materials [33,37,38], but has not been examined as a solid electrolyte for CO_2 sensing.

In this study, we focus on the performance and the limits of a CO_2 sensor using a Li_2CO_3 sensing electrode, $Li_{0.35}La_{0.55}TiO_3$ (LLTO) electrolyte and $Li_2TiO_3 + TiO_2$ reference electrode. Microstructure, electrical properties, and stability of the LLTO electrolyte in contact with lithium carbonate are presented, as well as conditions to optimize sensor performance.

2. Experimental

2.1. $Li_{0.35}La_{0.55}TiO_3$ (LLTO) electrolyte preparation and characterization

The electrolyte disk was prepared by a conventional solid-state reaction method. As starting materials, stoichiometric amounts of Li_2CO_3 (99.999%, Alfa Aesar), La_2O_3 (99.99%, Alfa Aesar), and TiO_2 (99.6%, Anatase, Alfa Aesar) were mixed in ethanol and the mixture was ball-milled for 20 h using a milling machine (PQ-N04). The milled mixture was dried at 100 °C in a convection oven followed by grinding in a mortar and pestle. The ground powder was calcined at 1100 °C for 12 h with 5 °C/min ramp rate in ambient atmosphere. After ball-milling, the powder was cold-pressed into green pellets of 6 mm diameter and 1 mm thickness. These green pellets were placed in a platinum crucible and heated to 1200 °C for 12 h with 3 °C/min ramp rate. At temperatures > 1200 °C, we noted phase segregation and melting, consistent with literature [38]. The sintered pellet was of final dimensions of about 5.4 mm in diameter and a thickness of about 0.9 mm.

The density of the sintered sample was determined from the Archimedes method using de-ionized water as the immersion fluid [39]. The phase identification was carried out by powder X-ray diffraction (XRD) method. The data was collected by a Rigaku X-ray diffractometer using Cu Kα radiation at 40 kV accelerating voltage and 25 mA current with a step size of 0.02° 2θ and counting time of 1 s. The microstructure of the sintered sample was observed using a scanning electron microscope (SEM, JEOL JSM-5500).

Electrical conductivity measurements were performed on the sintered sample; sputtered gold was formed as ion-blocking electrodes on the top and bottom sides of the pellet. Impedance was measured using a Solartron 1260A impedance analyzer in the frequency range from 1 Hz to 32 MHz with 100 mV ac applied voltage at temperatures between 25 °C and 550 °C in 21% O_2/N_2, 21% O_2/N_2 with 4000 ppm CO_2, and N_2 atmosphere, respectively. The electronic conductivity was examined by the Hebb–Wagner polarization method using a Gamry PC4/300; a gold ion blocking electrode was formed on one side of the pellet and a reversible electrode made from Li_2CO_3-gold particle mixture on the other side of the pellet. The tests were conducted at 300, 400, and 500 °C in 21% O_2/N_2 with 4000 ppm CO_2. The applied voltage varied from 0.05 to 1.4 V and the currents were monitored for 30 min at each voltage to obtain stead-state values. The detail of the Hebb–Wagner dc polarization method is described elsewhere [40].

To investigate the stability between the electrolyte and the sensing electrode, a mixture of $Li_{0.35}La_{0.55}TiO_3$ and Li_2CO_3 was heated for 2 h at 500, 600, and 700 °C in ambient air. To examine the stability at the interface between the electrolyte and the reference electrode, the reference materials (Li_2TiO_3 and TiO_2) were mixed with $Li_{0.35}La_{0.55}TiO_3$ and then were heated at 650 °C for 2 h in ambient air.

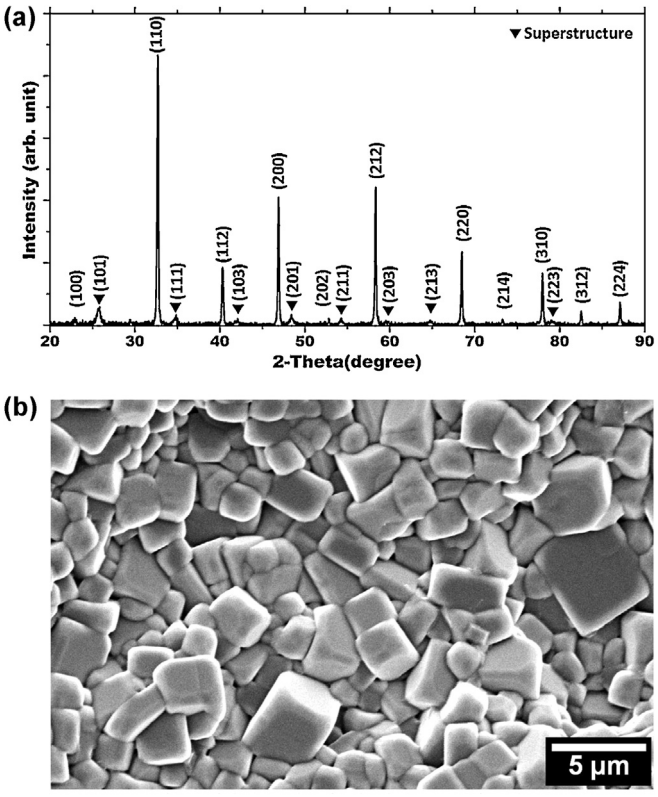

Fig. 1. (a) Powder X-ray diffraction pattern of $Li_{0.35}La_{0.55}TiO_3$ after sintering at 1200 °C for 12 h. (▼: Superstructure peaks indicative of tetragonal structure). (b) SEM image of $Li_{0.35}La_{0.55}TiO_3$ after sintering at 1200 °C for 12 h.

2.2. CO_2 Sensor fabrication

The sensor was composed of the following electrochemical cell:

$$CO_2,\ O_2,\ N_2|Li_2TiO_3 + 5\ wt\%\ TiO_2|Au|Li_{0.35}La_{0.55}TiO_3 |Au|Li_2CO_3|N_2,\ O_2,\ CO_2 \quad (1)$$

reference electrode |solid electrolyte (LLTO)| sensing electrode.

The details of the open reference electrode are described elsewhere [27,41,42]. The sensor was fabricated by the following procedure: i) gold contacts (Heraeus, C5789 or C5729) were formed on both sides of a sintered LLTO pellet by painting Au paste followed by a heat-treatment at 850 °C for 5–10 min; ii) to form the reference electrode, a mixture of 95 wt% Li_2TiO_3 (99%, Lithium Corporation of America Inc.), 5 wt% TiO_2 (99.6%, Anatase, Alfa Aesar) and α-terpinoel organic binder (Fisher Chemicals) was painted on one side of the electrolyte and was fired at 650 °C for 2 h; iii) to fabricate the sensing electrode, Li_2CO_3 powder (99% Alpha Aesar) mixed with α-terpinoel organic binder was painted on the other side followed by a heat-treatment in the temperature range between 350 and 700 °C for 2 h in ambient air.

2.3. Gas preparation and emf measurements

The concentration of CO_2 gas was controlled in the range between 500 and 4000 ppm by mixing nitrogen (99.99%), oxygen (50% balanced by N_2), and CO_2 (1% balanced by N_2). Total gas flow rate of the synthetic gas was 160 sccm and the background gas composition was maintained as 21% O_2/N_2. The CO_2 sensors were located in the middle of a quartz tube inside a Lindberg Blue M furnace and the tests were conducted at temperatures ranging from 300 to 550 °C under dry condition. The emf was measured by an HP 34970A data acquisition system and was recorded by Agilent

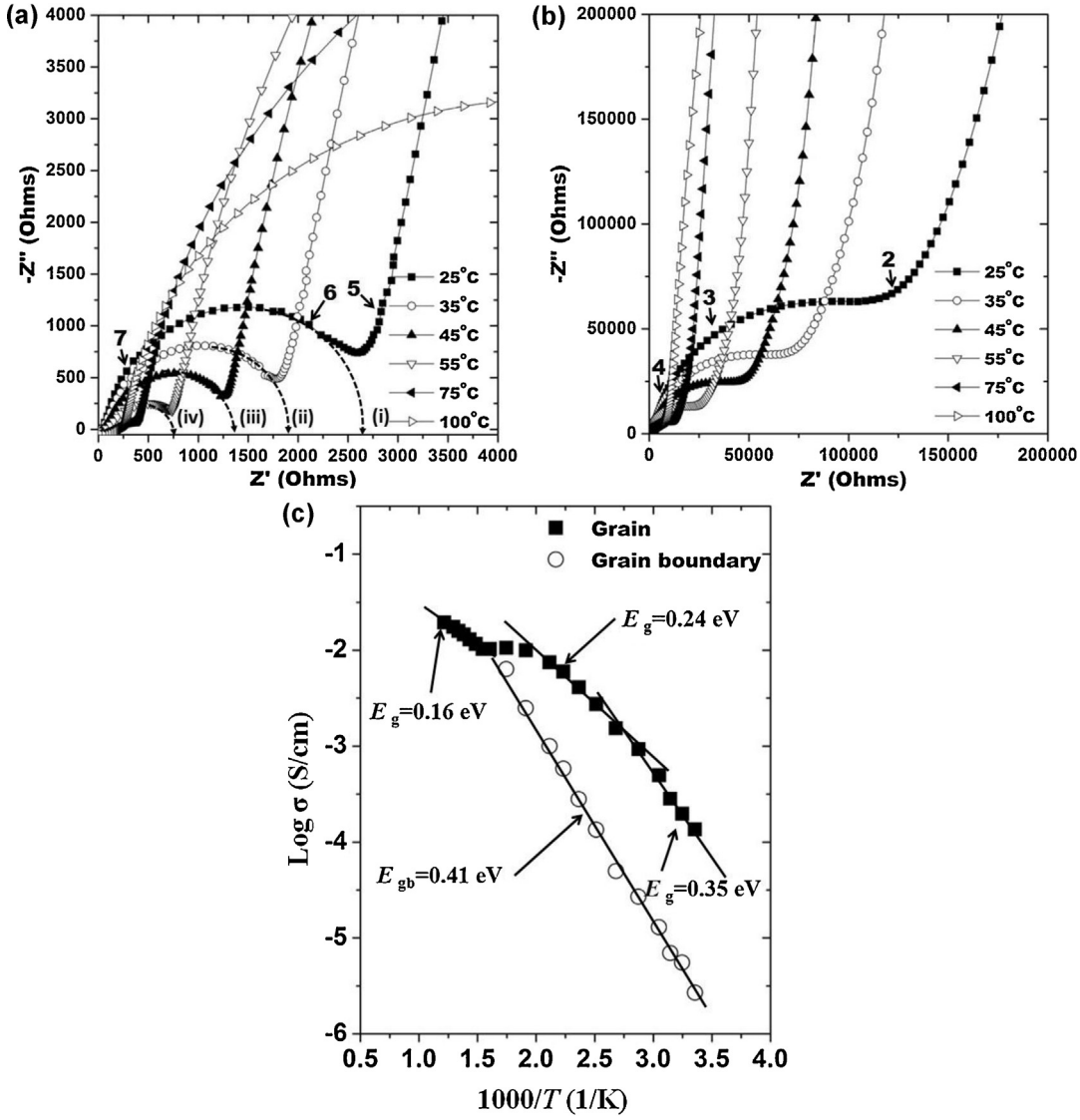

Fig. 2. (a) High frequency region (32–0.1 MHz) of the impedance plots of the sintered $Li_{0.35}La_{0.55}TiO_3$ as a function of temperature (25–100 °C). The impedance was measured in N_2 atmosphere (Numbers in the figure correspond to exponent of 10 in frequency, Hz). (b) Low frequency region (0.1 MHz-100 Hz) of the impedance plots of the sintered $Li_{0.35}La_{0.55}TiO_3$ as a function of temperature (25–100 °C). The impedance was measured in N_2 atmosphere (numbers in the figure correspond to exponent of 10 in frequency, Hz). (c) Arrhenius plots of the conductivity of sintered pellet of $Li_{0.35}La_{0.55}TiO_3$, ■: grain region, ○: grain boundary region.

BenchLink Data Logger 3 (Ver.3.10.00). The data was collected every 5 s. The performances of the sensors were judged from the percent Nernstian behavior. The magnitude of emf change from the baseline (21% O_2/N_2) to the steady state potential at each CO_2 concentration was estimated, and was defined as the sensor response. The theoretical EMF obtained based on Eq. (1) is shown in Eq. (2).

$$\mathrm{EMF} = E^0 + \frac{2.303RT}{2F} \log\ p(\mathrm{CO_2}) \tag{2}$$

where R is the gas constant, T temperature, F Faraday's constant, and E^0 is the standard potential, respectively [27]. The theoretical slope at a temperature T is $2.303RT/2F$. Based on the observed sensor responses, the emf change was plotted against the CO_2 partial pressure, and the slope for the experimental data was calculated. The percent Nernstian behavior was defined as:

$$\text{Percent Nernstian behavior} = 100 \times \frac{\text{slope from measured values}}{\text{slope from theoretical values}} \tag{3}$$

3. Results

3.1. Characterization of $Li_{0.35}La_{0.55}TiO_3$ (LLTO)

Fig. 1(a) shows the XRD pattern of LLTO powders prepared from a mixture of Li_2CO_3, La_2O_3, and TiO_2 by heating at 1200 °C for 12 h. All diffraction peaks can be indexed to LLTO having tetragonal (*P4/mmm*) structure (JCPDS #87-0935), and is consistent with literature [43,44]. This structure is the result of double stacking of the perovskite cubic unit cell along the c-axis with ordering of La^{3+}, Li^+, and vacancies (the superstructure peaks are marked with an inverse triangle) [33,44].

The microstructure of the sintered LLTO pellet is shown in Fig. 1(b), with grains of "rectangular" cubic shapes with minimal overall porosity. The average grain size was calculated as 1.5–1.6 μm (linear intercept method). The measured density of the sintered LLTO is 4.76 g/cm^3, 94% of the theoretical value (5.02 g/cm^3).

Fig. 2 shows the impedance data between 25 and 100 °C in nitrogen atmosphere for the sintered LLTO pellet with sputtered

Au electrodes. It was possible to distinguish a high frequency (32–0.1 MHz, Fig. 2(a)) semicircle and a low frequency semicircle (10^5–10^2 Hz, Fig. 2(b), the numbers in the figures indicate the exponent of 10 in frequency (Hz)), and correlated with grain (high frequency) and grain boundary conductivities (low frequency), respectively [45]. Upon increasing the measurement temperature, the intercept of the semicircles on the Z'-axis decreased from (i) to (iv) as shown in Fig. 2(a). It was difficult to identify the high frequency circle above 100 °C, due to reduction of the grain resistance.

The grain and grain boundary conductivity of the sintered LLTO was calculated based on a simple equivalent circuit model. From 25 to 100 °C the impedance data was fitted with two RC circuits in series, since two semicircles were clearly observed. Between 100 and 300 °C, only the semicircle due to the grain boundary is discernible. So, the grain conductivity was chosen from where the curve intercepted the Z' axis at high frequency and the grain boundary from the fitting to a single RC circuit. Beyond 300 °C, the grain boundary semicircle was not discernible (the curvature in the impedance plot was no longer obvious in the frequency range measured), so only the grain conductivity was determined from the intercept on the Z' axis. At 25 °C, the value of the grain conductivity was estimated to be 1.35×10^{-4} S/cm, while that for the grain boundary was 2.69×10^{-6} S/cm (using dimensions of the sample), with the latter dominating the total conductivity of LLTO. These values are in good agreement with those reported in literature [43,46,47].

Fig. 2(c) shows the Arrhenius plots of the grain and grain boundary conductivities of LLTO as a function of temperature. The plot for grain conductivity exhibits a change in the slope at temperatures of 100, 250, and 375 °C, whereas the plot for grain boundary does not. The activation energy for grain boundary conduction was 0.41 eV from 25 to 300 °C and agrees well with literature [33]. From Fig. 2(c), it is possible to get 3 different activation energies for grain conduction: 0.35 eV for 25 °C < T < 100 °C, 0.24 eV for 100 °C < T < 250 °C, a transition region 250 °C < T < 375 °C, and 0.16 eV for 375 °C < T. This phenomenon has been noted before, and explanations include a phase transition [33,48], or a change in conduction mechanism at higher temperature (T > 127 °C) arising from tilting or rotating of the TiO_6 octahedra [34,37].

For the Hebb–Wagner polarization measurement, the sample was constructed as follows:

$$(-)\,\text{a mixture of } Li_2CO_3 + \text{Au particles}|Li_{0.35}La_{0.55}TiO_3|\text{Au}\,(+) \quad (4)$$

A mixture of Li_2CO_3 + Au particles and Au were used as a reversible electrode and ion-blocking electrode, respectively. Fig. 3 presents the change in the current density with applied potential at 300, 400, and 500 °C (inset). As the applied voltage was increased, the current density reached a plateau and subsequently increased again. The voltage–current density curve from Hebb–Wagner polarization can be separated into the electron and hole currents [40]:

$$J_n = \sigma_n \left[1 - \exp\left(-\frac{EF}{RT}\right)\right]\left(\frac{RT}{LF}\right) \quad (5)$$

$$J_p = \sigma_p \left[\exp\left(\frac{EF}{RT}\right) - 1\right]\left(\frac{RT}{LF}\right) \quad (6)$$

where L is the thickness of the sample, R gas constant, E the potential, F Faraday's constant, and σ_n and σ_p are the conductivities due to electrons and holes, respectively. From the steady state (plateau) value in Fig. 3, n-type electronic conductivity of LLTO can be estimated using Eq. (5). The calculated electronic conductivity and transference number for lithium ion are given in Table 1. The transference number for lithium ion conduction (t_{Li+}) is calculated as

$$t_{Li^+} = \frac{\sigma_{Li^+}}{\sigma_{Li^+} + \sigma_n} \quad (7)$$

Total ionic conductivity was used for calculating the transference number in Eq. (7). Since it was not possible to get grain-boundary conductivity for LLTO in the temperature range between 300 and 500 °C, the linear curve shown in Fig. 2(c) was extrapolated to 500 °C, and the values obtained were added to the grain conductivity to get a total value. The calculation confirmed that the solid electrolyte LLLTO has almost negligible n-type electronic conductivity from 300 to 500 °C, consistent with literature [34].

Table 1
Electronic conductivity, total conductivity, and lithium ionic transference number calculated from Hebb–Wagner method for $Li_{0.35}La_{0.55}TiO_3$.

	Electronic conductivity (S/cm)	Total conductivity (S/cm)	Transference number for lithium ion (t_{Li+})
300 °C	3.03×10^{-6}	3.97×10^{-3}	0.9992
400 °C	5.79×10^{-6}	7.21×10^{-3}	0.9992
500 °C	3.24×10^{-5}	1.27×10^{-2}	0.9975

3.2. Reactivity of $Li_{0.35}La_{0.55}TiO_3$ (LLTO)

3.2.1. With Li_2CO_3 sensing electrode

Mixtures of $Li_{0.35}La_{0.55}TiO_3$ and Li_2CO_3 powders were heated at 500, 600, and 700 °C for 2 h in ambient air and Fig. 4 show the resulting XRD patterns. With heat-treatment at 500 °C (Fig. 4(b)), no new peaks were detected and all peaks were assigned to LLTO (▼, JCPDS #87-0935) and Li_2CO_3 (●, JCPDS #87-0728). As temperature increased to 600 °C (Fig. 4(c)), the intensities of (1 0 1), (1 1 0), (1 1 2), (2 0 0), and (2 1 2) peaks of LLTO were reduced. At 700 °C (Fig. 4(d)), the peaks from Li_2CO_3 and LLTO almost disappeared and the new peaks are still characteristic of a perovskite structure. Fig. 4(e) shows that the compound synthesized (procedure similar to LLTO) with the composition $Li_{1.75}La_{0.55}TiO_3$ has a similar diffraction pattern to the material formed at 700 °C. The morphological

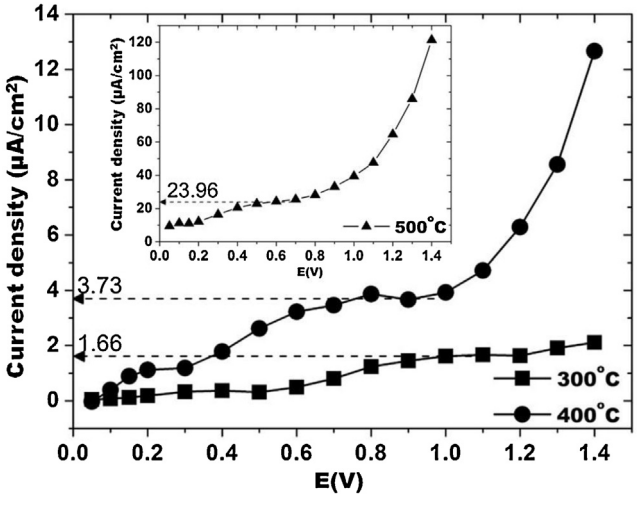

Fig. 3. Hebb–Wagner polarization curve for sintered $Li_{0.35}La_{0.55}TiO_3$; current density is computed at each voltage from steady state current. The test was conducted in 21% O_2/N_2 in 4000 ppm CO_2 atmosphere (dashed lines correspond to the n-type electronic current density).

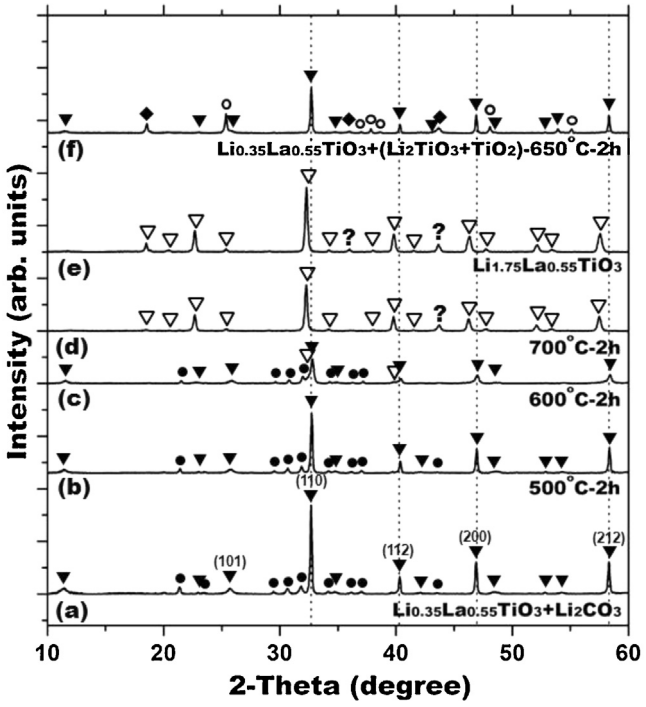

Fig. 4. XRD patterns after heating (a) a mixture of $Li_{0.35}La_{0.55}TiO_3$ and Li_2CO_3 at (b) 500, (c) 600, (d) 700 °C for 2 h in ambient air, (e) lithium excess $Li_{1.75}L_{0.55}TiO_3$ prepared at 1100 °C for 12 h, and (f) a mixture of $Li_{0.35}La_{0.55}TiO_3$ and $Li_2TiO_3$and TiO_2 heated at 650 °C for 2 h in ambient air (▼: $Li_{0.33}La_{0.557}TiO_3$, ●: Li_2CO_3, ▽: $LaLi_{1/3}Ti_{2/3}O_3$, ♦: Li_2TiO_3, ○: TiO_2 (anatase), and?: unassigned).

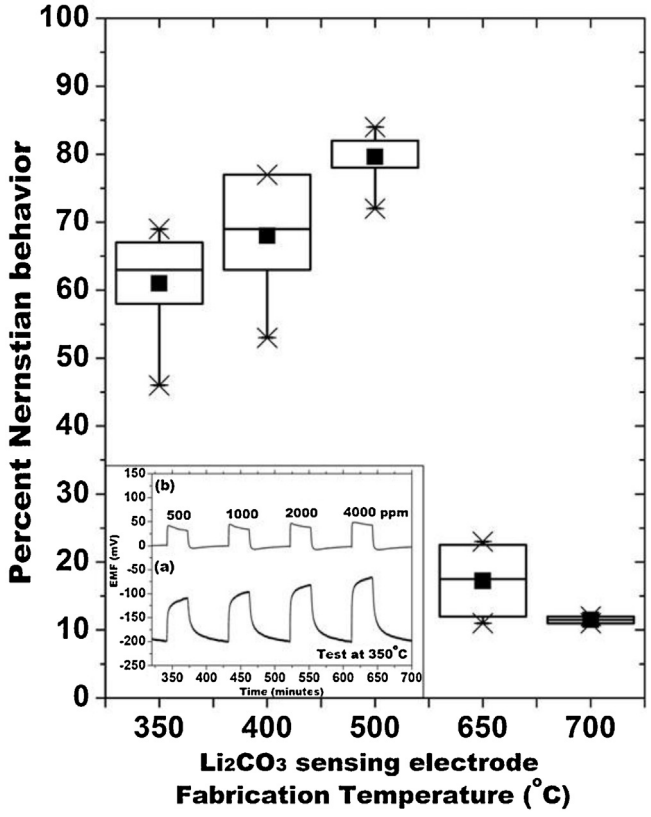

Fig. 5. Percent of Nernstian behaviors at 350 °C versus fabrication temperature of Li_2CO_3 sensing electrode on $Li_{0.35}La_{0.55}TiO_3$ (reference electrode was fabricated at 650 °C for 2 h prior to deposition of Li_2CO_3 sensing electrode) Inset: CO_2 sensing time traces of LLTO sensor with Li_2CO_3 sensing electrode fabricated at (a) 500, and (b) 700 °C-2 h, respectively.

changes also suggest a reaction between LLTO and Li_2CO_3, and are shown in Supplementary Section.

3.2.2. Li_2TiO_3 and TiO_2 reference electrode materials

Mixtures of LLTO, Li_2TiO_3, and TiO_2 were heated at 650 °C for 2 h in air. As shown in Fig. 4(f), XRD results of the powders exhibited no new peaks indicating that $Li_2TiO_3 + TiO_2$ reference material is stable in contact with LLTO at 650 °C.

3.3. $Li_{0.35}La_{0.55}TiO_3$ based CO_2 (LLTO) sensor

Fig. 5 compares the percent Nernstian behavior calculated from the sensor response at 350 °C for several samples in which the sensing electrode Li_2CO_3 on LLTO was fabricated at 350, 400, 500, 650, and 700 °C for 2 h in air (the reference electrode was first assembled at 650 °C). As the fabrication temperature of sensing electrode increased from 350 to 500 °C, the sensor performance improved (67% to 81%). However, as the sensing electrode was fabricated above 500 °C, *e.g.* 650 and 700 °C, the percent Nernstian value dropped to 17% and 11%, respectively. An inset in Fig. 5 shows the actual transients upon change of CO_2 gas concentrations (500, 1000, 2000, and 4000 ppm) at 350 °C test for the sensors prepared at 500 and 700 °C. For the sensor with 500 °C (inset a), the emf response transients changed with CO_2. For the sensor prepared at 700 °C (inset b), in contrast, the emf exhibited very little change with CO_2 concentration.

Since the devices prepared with the sensing electrode fabricated at 500 °C in air produced the optimal CO_2 sensing performance, more detailed studies as a function of sensing temperature were carried out with sensors fabricated at this temperature. The sensor traces and the percent Nernstian value of the sensor are shown in Fig. 6(a) and (b), respectively. The tests were carried out in 21% O_2/N_2 background gas and the concentration of CO_2 was varied from 500 to 4000 ppm or from 1000 to 4000 ppm (Fig. 6(b)). This sensor approached 62% of theoretical value at 300 °C, and improved to almost ideal Nernstian behavior (90–98%) in the temperature range of 425–450 °C. The response/recovery times also improved with temperature, the data at 450 °C indicates a response time of 1 min and recovery of 4 min (t_{90} in both cases). After testing at 500–550 °C, the sensor was examined again at 350 °C, but it was irreversibly degraded (data not shown).

3.4. Sensor interferences from other gas species

In Fig. 7(a), the sensing traces for 1000 ppm CO_2 measured at 400 °C in differing oxygen backgrounds are presented. There is a slight change in baseline (~10 mV) with change of O_2 concentration from 21 to 16%, as compared to a ~250 mV signal for CO_2. The interference with humidity is more pronounced and shown in Fig. 7(b). There is a decrease in signal with 100% humidity in the gas stream, for 1000 ppm CO_2, the decrease is of the order of 30%, though the percent Nernstian behavior is similar in the dry and humid cases.

4. Discussion

4.1. Sensor performance

The sensor performance is expected to follow Eq. (2), as long as LLTO is a pure lithium ionic conductor, as verified by the Hebb–Wagner measurements (Fig. 3, Table 1). Fabrication of the sensor devices involved heat treatment of the LLTO with Li_2CO_3 (sensing) and $Li_2TiO_3 + 5$ wt% TiO_2 (reference) at temperatures

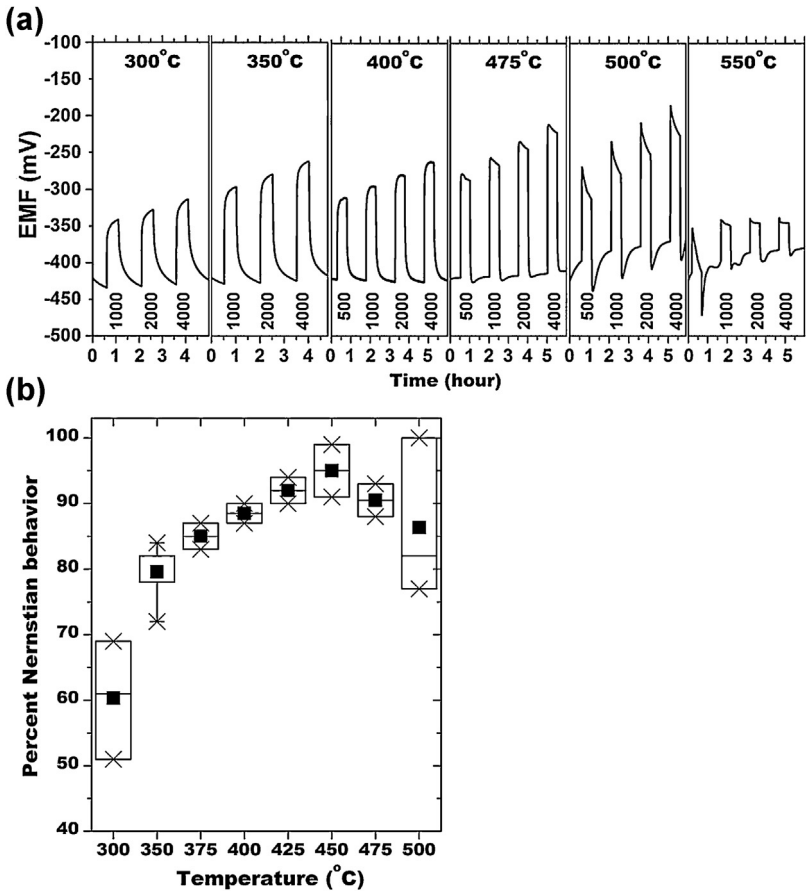

Fig. 6. (a) CO_2 sensing time traces from 300 to 550 °C of $Li_{0.35}La_{0.55}TiO_3$ sensor with Li_2CO_3 sensing electrode (fabricated at 500 °C 2 h in air) in 21% O_2/N_2 background gas. The numbers below traces are CO_2 concentration in ppm. (b) The change of percent Nernstian behavior for the $Li_{0.35}La_{0.55}TiO_3$ based CO_2 sensor with Li_2CO_3 sensing electrode fabricated at 500 °C for 2 h in air depending on test temperature; test in 21% O_2/N_2 background.

ranging from 500 to 700 °C. There is no chemical reaction between LLTO and the reference electrode materials (Fig. 4(f)).

However, when mixtures of $Li_{0.35}La_{0.55}TiO_3$ and Li_2CO_3 were heated, there were changes in the XRD powder patterns beginning at 600 °C (Fig. 4(c)). Morphological examination of the surface also exhibited changes beginning at 600 °C (Supplementary Section). Thus, there are indications that Li_2CO_3 and LLTO are reacting at temperatures ≥600 °C in air. The pattern at 700 °C is assigned to $LaLi_{1/3}Ti_{2/3}O_3$ formed by insertion of excess Li^+ into LLTO [49–51]. Support for this hypothesis also comes from the XRD of $Li_{1.75}La_{0.55}TiO_3$ which was prepared by heating the corresponding amounts of Li_2CO_3 (excess), La_2O_3, and TiO_2 at 1100 °C (12 h) (compare Fig. 4(e) and (d)). These results explain why sensor performance was poor at temperatures > 600 °C.

However, what is puzzling is that there is no obvious reaction between LLTO and Li_2CO_3 at 500 °C during 2 h in air (Fig. 4(b)), yet sensing tests indicated that sensor performance permanently deteriorated above 475 °C (Fig. 6). Li_2CO_3 can decompose via the following reaction:

$$Li_2CO_3(s) \rightarrow Li_2O(s) + CO_2(g) \quad (8)$$

and indicates that at low partial pressures of CO_2, the decomposition of Li_2CO_3 will be favored. The ΔG of reaction (8) at various temperatures and CO_2 partial pressures are presented in Fig. 8(a). At a fixed temperature, the ΔG becomes more negative as the CO_2 partial pressure decreases. Around 495 °C, the equilibrium CO_2 partial pressure for reaction (8) is calculated as 100 ppb. In this study, the background gas (21% O_2/N_2) was synthesized by mixing 50% O_2/N_2 and 99.99% N_2 and thus the level of CO_2 in the background gas would be at low ppb level, indicating that from thermodynamic considerations, reaction (8) can indeed occur.

To confirm that LLTO reacts with Li_2CO_3 at 500 °C in the absence of CO_2, a mixture of LLTO and Li_2CO_3 was heated at 500 °C for 55 h with/without 4000 ppm CO_2. As presented in Fig. 8(b), no additional phase was identified for the mixture heated in the presence of 4000 ppm CO_2. However the XRD patterns in the absence of CO_2, the diffraction peaks from $Li_{0.33}L_{0.557}TiO_3$ disappeared. We propose that at low levels of CO_2, Li_2CO_3 can decompose and the resulting Li_2O reacts with the surface of the sintered LLTO electrolyte, filling Li^+ vacancies and interstitials, and altering its electrical properties leading to sensor degradation. Literature reports indicate that the kinetics for Eq. (8) is slow, even at low partial pressures of CO_2, and the decomposition reaction is promoted by the presence of other solids, such as silica [52]. In this study, LLTO could be serving in that capacity.

For further proof of the relevance of reaction (8), two sensor devices were heated at 500 °C for 72 h with and without CO_2 (4000 ppm) in 21% O_2/N_2 background atmosphere, respectively. After the heat-treatment, the sensors were tested at 350 °C. As presented in Fig. 8(b) (inset), the sensor heated in presence of CO_2 shows sensing performance with 85% of Nernstian value and the baseline is stable. The device fabricated in the absence of CO_2, however, showed very poor sensing characteristics.

4.2. Practical Implications of Sensor Fabrication and Performance

Based on reaction (8), introduction of high concentration of CO_2 (~99.99%) will minimize reaction between Li_2CO_3 and LLTO

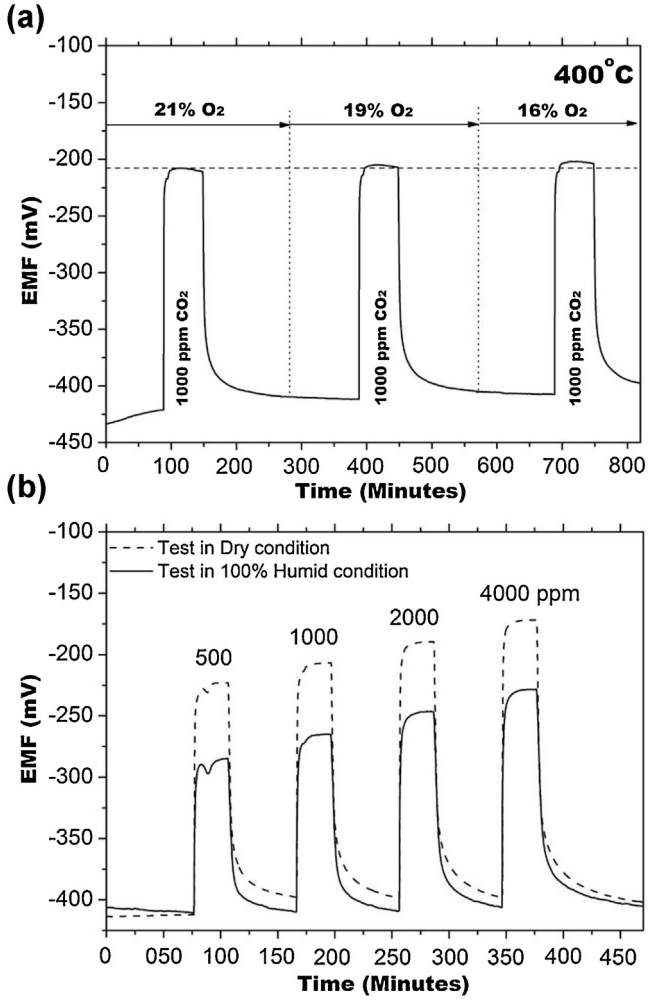

Fig. 7. (a) Response transients to 1000 ppm CO_2 at 400 °C of $Li_{0.35}La_{0.55}TiO_3$ sensor with Li_2CO_3 sensing electrode (fabricated at 500 °C 2 h in air) in 21, 19, and 16% O_2/N_2 background gas. (b) CO_2 sensing time traces in 100% humid condition (bold line) and in dry condition (dashed line) at 400 °C of $Li_{0.35}La_{0.55}TiO_3$ sensor with Li_2CO_3 sensing electrode (fabricated at 500 °C 2 h in air) in 21% O_2/N_2 background gas.

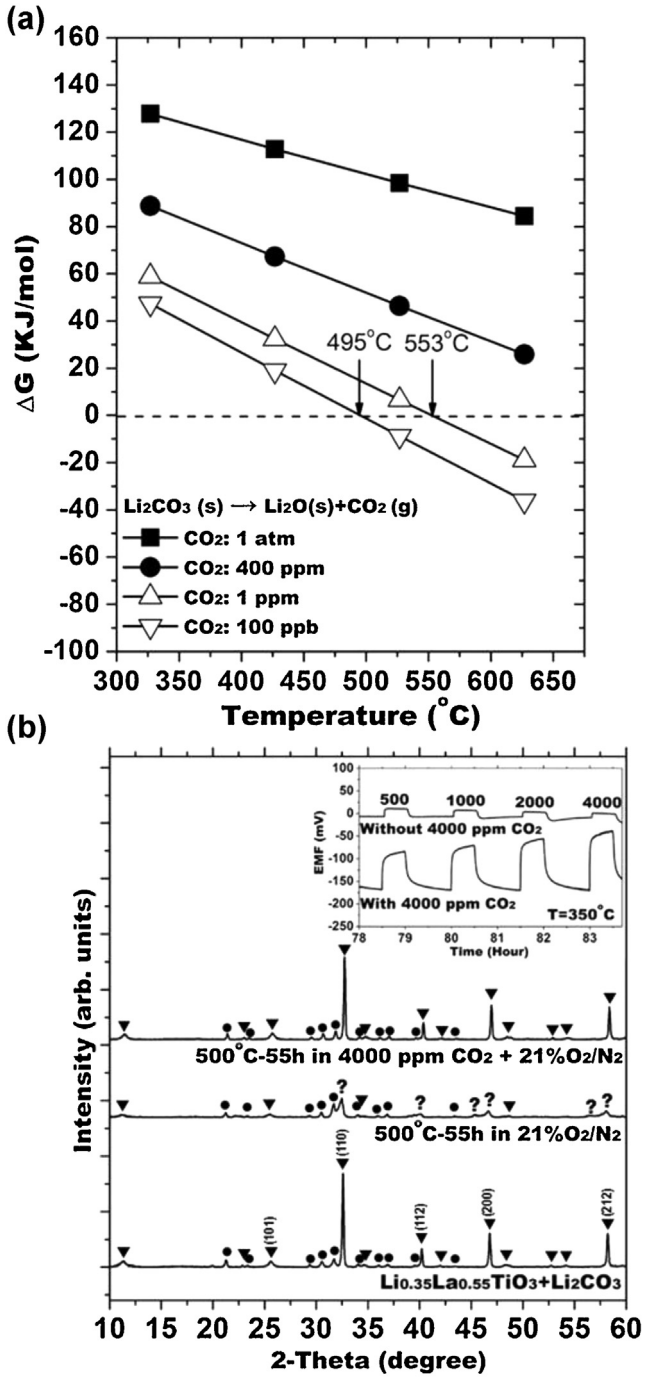

Fig. 8. (a) Calculated ΔG (free energy) with varying CO_2 partial pressure for Li_2CO_3 decomposition. (b) XRD pattern of $Li_{0.35}La_{0.55}TiO_3$-Li_2CO_3 mixture and change after heat-treatment at 500 °C for 55 h in CO_2 free 21% O_2/N_2 and 4000 ppm CO_2 in 21% O_2/N_2; inset: CO_2 sensing time traces of $Li_{0.35}La_{0.55}TiO_3$ based CO_2 sensor with Li_2CO_3 treated with/without 4000 ppm CO_2 for 72 h (▼: $Li_{0.33}La_{0.557}TiO_3$, ●: Li_2CO_3, and?: unassigned).

even at high temperatures, and provides an opportunity for high temperature fabrication, which will improve bonding between the electrode and the electrolyte. Fig. 9 shows significant improvement of the sensor fabricated at 650 °C by introducing 99.99% CO_2 during the fabrication (◯), whereas the sensor fabricated in air showed poor response (●) (percent Nernstian value increased from 20% to 80% at 350 °C and from 18% to 85% at 375 °C).

For practical long-term sensor operation, the presence of CO_2 in the environment will prolong long term operation of the sensor temperature. Fig. 10(a) and (b) shows CO_2 sensing responses over long periods at 475 °C with and without background 400 ppm CO_2 (mimicking an ambient environment) respectively. In the absence of background CO_2, the sensor's performance degraded. In the presence of background CO_2, the baseline drifted 25 mV during a week and the percent Nernstian value changed from 91% to 88% (practically within experimental error). Thus, ~400 ppm CO_2 in the background is enough to keep reaction (8) from happening and stabilizing the sensor response. Therefore the sensor system as outlined in this study based on $Li_{0.35}La_{0.55}TiO_3$-Li_2CO_3 will be suitable for detecting changes of CO_2 in ambient air, or other high CO_2 environments such as combustion processes, but will not be appropriate for long term sensing measurements in zero CO_2 background environments.

4.3. Limitations due to interferences

The sensor exhibits minimal interference to oxygen (Fig. 7(a)), as expected, since according to Eq. (2), there is no dependence on oxygen concentration for the sensor signal, since both the reference and sensor electrode are exposed to the same gas. However, with humidity, there is considerable interference (Fig. 7(b)). We have not examined the origin of this interference, but it is reported in the literature that LLTO will react with water [53].

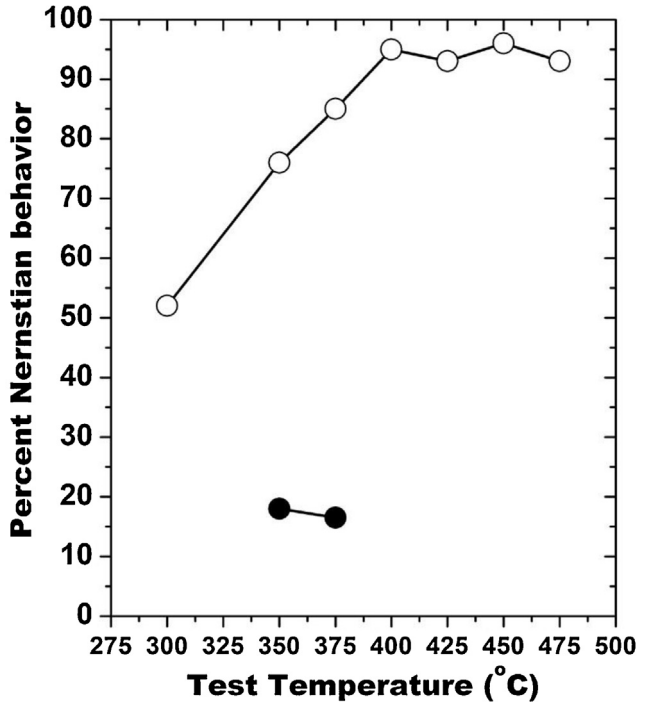

Fig. 9. Percent of Nernstian behaviors of the sensors with Li_2CO_3 fabricating at 650 °C-2 h in 99.99% CO_2 (○) and at 650 °C-2 h in air (●); tests in 21% O_2/N_2 atmosphere.

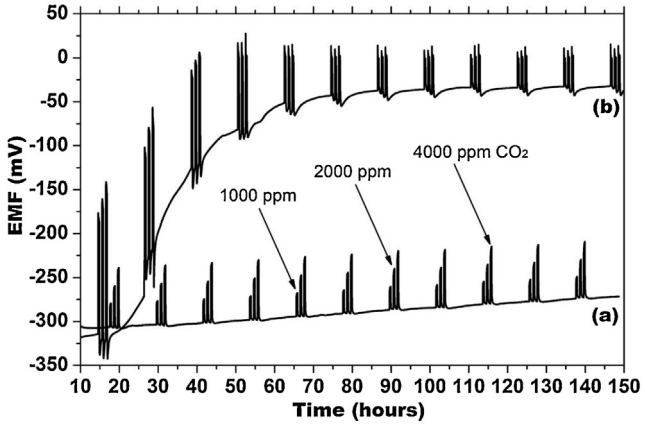

Fig. 10. Long term stability of the $Li_{0.35}La_{0.55}TiO_3$ sensor at 475 °C in (a) 21% O_2/N_2 and (b) 400 ppm +21% O_2/N_2; sensors fabricated (a) at 650 °C for 2 h in 99.99% CO_2 and (b) at 500 °C for 2 h in air.

5. Conclusions

A potentiometric CO_2 gas sensor with $Li_{0.35}La_{0.55}TiO_3$ (LLTO) electrolyte was examined with Li_2CO_3 sensing electrode and $Li_2TiO_3 + TiO_2$ reference electrode. $Li_{0.35}La_{0.55}TiO_3$ was confirmed to behave as a low temperature Li^+ conductor. It was revealed that LLTO electrolyte reacts with Li_2CO_3 and the crucial factors of this reaction are temperature and CO_2 partial pressure in the reaction environment. At temperatures exceeding 600 °C, the LLTO-Li_2CO_3 reaction leads to formation of $LaLi_{1/3}Ti_{2/3}O_3$ which changes the electrical properties, and sensors designed at these temperatures exhibit poor performance. At 500 °C, under environments with low CO_2 concentrations (ppb), Li_2CO_3 reacts with LLTO via insertion of Li^+ into the vacancies, and interstitials. Sensors at 500 °C eventually degrade as the interface reaction occurs. With this knowledge, we fabricated sensors at 650 °C in the presence of high concentrations of CO_2 that prevented the LLTO-Li_2CO_3 reaction and improved sensor performance. However, for long-term practical application of these sensors, CO_2 needs to be present in the measuring environment. For example, this sensor can be used to monitor fluctuations in CO_2 in the ambient atmosphere in the temperature range of 300–450 °C, and also for measuring changes of CO_2 in combustion streams. The sensors will eventually degrade if they are used in zero CO_2 background environments.

Acknowledgement

We acknowledge funding from NASA for this research.

Appendix A. Supplementary data

Supplementary data associated with this article can be found, in the online version, at http://dx.doi.org/10.1016/j.snb.2013.02.104.

References

[1] T.M.L. Wigley, The pre-industrial carbon dioxide level, Climatic Change 5 (1983) 315–320.
[2] W.J. Manning, A.V. Tiedemann, Review paper—climate change: potential effects of increased atmospheric carbon dioxide (CO_2), ozone (O_3), and ultraviolet-B (UV-B) radiation on plant dieases, Enviromental Pollution 88 (1995) 219–245.
[3] G.W. Hunter, R.A. Dweik, Applied breath analysis: an overview of the challenges and opportunities in developing and testing sensor technology for human health monitoring in aerospace and clinical applications, Journal of Breath Research 2 (2008) 037020.
[4] S.-J. Chen, D.C. Hovde, K.A. Peterson, A.W. Marshall, Fire detection using smoke and gas sensors, Fire Safty Journal 42 (2007) 507–515.
[5] S.A. Akbar, P.K. Dutta, C. Lee, High-temperature ceramic gas sensors: a review, International journal of Applied Ceramic Technology-Ceramic Product Development and Commercialization 3 (2006) 302–311.
[6] J. Zosel, W. Oelβner, M. Decker, G. Gerlach, U. Guth, The measurement of dissoved and gaseous carbon dioxide concentration, Measurement Science and Technology 22 (2011) 45, 072001.
[7] W. Weppner, R.A. Huggins, Electrochemical methods for determining kinetics properties of solids, Annual Review Materials Science 8 (1978) 269–311.
[8] D.L. Auble, T.P. Meyers, An open path, fast response infrared absorption gas analyzer for H_2O and CO_2, Boundary-Layer Meterology 59 (1992) 243–256.
[9] M. Holzinger, J. Maier, W. Sitte, Potentiometric detection of complex gases: application to CO_2, Solid State Ionics 94 (1997) 217–225.
[10] M. Mulier, V. Zeninary, L. Joly, T. Decarpenterie, B. Parvitte, P. Jeandet, G. Liger-Belair, Development of a compact CO_2 sensor based on near-infrared laser technology for enological application, Applied Physics B-Lasers and Optics 94 (2009) 725–733.
[11] N. Yamazoe, N. Miura, Prospect and problems of solid electrolyte-based oxygenic gas sensors, Solid State Ionics 86–88 (1996) 987–993.
[12] J.W. Fergus, A review of electrolyte and electrode materials for high temperature electrochemical CO_2 and SO_2 gas sensors, Sensors and Actuators B: Chemical 134 (2008) 1034–1041.
[13] T. Kida, K. Shimanoe, N. Miura, N. Yamazoe, Stability of NASICON-based CO_2 sensor under humid conditions at low temperatures, Sensors and Actuators B 75 (2001) 179–187.
[14] P. Pasierb, S. Komornicki, S. Koziński, R. Gajerski, M. Rękas, Long-term stability of potentiometric CO_2 sensors based on Nasicon as a solid electrolyte, Sensors and Actuators B 101 (2004) 47–56.
[15] Y. Sadaoka, NASICON based CO_2 gas sensor with an auxiliary electrode composed of Li_2CO_3-metal oxide mixtures, Sensors and Actuators B 121 (2007) 194–199.
[16] Y. Shimamoto, T. Okamoto, H. Aono, L. Montanaro, Y. Sadaoka, Deterioration of phenomena of electrochemical CO_2 sensor with Pt, Na_2CO_3/Na_2O-Al_2O_3-$4SiO_2$//YSZ/Pt structure, Sensors and Actuators B 99 (2004) 141–148.
[17] Y. Shimamoto, T. Okamoto, Y. Itagaki, H. Aono, Y. Sadaoka, Performance and stability of potentiometric CO_2 gas sensor based on the Pt, Li_2CO_3/Na_2O-Al_2O_3-$4SiO_2$//YSZ/Pt electrochemical cell, Sensors and Actuators B 99 (2004) 113–117.
[18] T. Okamoto, Y. Shimamoto, N. Tsumura, Y. Itagaki, H. Aono, Y. Sadaoka, Drift phenomena of electrochemical CO_2 sensor with Pt, Na_2CO_3/Na+-electrolyte//YSZ/Pt structure, Sensors and Actuators B 108 (2005) 346–351.
[19] K. Obata, S. Matsushima, Relationship between aging time and EMF change of potentiometric CO_2 device using $Na_{1+x}Zr_2Si_xP_{3-x}O_{12}$ ($0 < x < 3$), Sensors and Actuators B 139 (2009) 435–439.
[20] K. Obata, S. Matsushima, CO_2 sensing performances of potentiometric sensor based on $Na_{1+x}Zr_2Si_2PO_{12}$ ($0 < x < 3$), Journal of the Ceramic Society of Japan 118 (2010) 213–216.
[21] N. Imanaka, T. Kawasato, G.-y. Adachi, A Carbon dioxide gas sensor probe based on a lithium ionic conductor, Chemistry Letters 19 (1990) 497–500.
[22] N. Imanaka, T. Murata, T. Kawasato, G.-y. Adachi, CO_2 detection with lithium solid electrolyte sensors, Sensors and Actuators B 13–14 (1993) 476–479.

[23] H. Narita, Z.Y. Can, J. Mizusaki, H. Tagawa, Solid state CO_2 sensor using an electrolyte in the system Li_2CO_3-Li_3PO_4-Al_2O_3, Solid State Ionics 79 (1995) 349–353.
[24] Y.C. Zhang, H. Tagawa, S. Asakura, Solid-state CO_2 sensor with Li_2CO_3-Li_3PO_4-$LiAlO_2$ electrolyte and $LiCoO_2$-Co_3O_4 as solid reference electrode, Journal of The Electrochemical Society 144 (1997) 4345–4350.
[25] F. Salam, P. Birke, W. Weppner, Solid-state CO_2 sensor with Li_2CO_3-MgO electrolyte and $LiMn_2O_4$ as solid reference electrode, Electrochemical and Solid-State Letters 2 (1999) 201–204.
[26] M.-G. Seo, B.-H. Kang, Y.-S. Chai, K.-D. Song, D.-D. Lee, CO_2 gas sensor using lithium ionic conductor with inside heater, Sensors and Actuators B 65 (2000) 346–348.
[27] C. Lee, P.K. Dutta, R. Ramamoorthy, S.A. Akbar, Mixed ionic and electronic conduction in Li_3PO_4 electrolyte for a CO_2 gas sensor, Journal of The Electrochemical Society 153 (2006) H4–H14.
[28] C. Lee, S.A. Akbar, C.O. Park, Potentiometric CO_2 gas sensor with lithium phosphorous oxynitride electrolyte, Sensors and Actuators B 80 (2001) 234–242.
[29] Y.C. Zhang, M. Kaneko, K. Uchida, J. Mizusaki, H. Tagawa, Solid electrolyte CO_2 sensor with lithium ion conductor and Li transition metal complex oxide as solid reference electrode, Journal of The Electrochemical Society 148 (2001) H81–H84.
[30] M. Matsui, Carbon Dioxide gas sensor with Li_2TiSiO_5 Solid electrolyte and NiO-Li_2CO_3 as sensing electrode, Journal of the Ceramic Society of Japan 111 (2003) 848–851.
[31] I. Lee, S.A. Akbar, P.K. Dutta, High temperature potentiometric carbon dioxide sensor with minimal interference to humidity, Sensors and Actuators B 142 (2009) 337–341.
[32] V. Thangadurai, W. Weppner, Recent progress in solid oxide and lithium ion conducting electrolytes research, Ionics 12 (2006) 81–92.
[33] Y. Inaguma, C. Liquan, M. Itoh, T. Nakamura, T. Uchida, H. Ikuta, M. Wakihara, High ionic conductivity in lithium lanthanum titanate, Solid State Communications 86 (1993) 689–693.
[34] S. Stramare, V. Thangadurai, W. Weppner, Lithium lanthanum titanates: a review, Chemistry of Materials 15 (2003) 3974–3990.
[35] O. Bohnke, The fast lithium-ion conducting oxides $Li_{3x}La_{2/3-x}TiO_3$ from fundamentals to application, Solid State Ionics 179 (2008) 9–15.
[36] S. Kunugi, Y. Inaguma, M. Itoh, Electrochemical recovery and isotope separation of lithium ion employing lithium ion conductive perovskite-type oxides, Solid State Ionics 122 (1999) 35–39.
[37] O. Bohnke, C. Bohnke, J.L. Fourquet, Mechanism of ionic conduction and electrochemical intercalation of lithium into the perovskite lanthanum lithium titanate, Solid State Ionics 91 (1996) 21–31.
[38] C.H. Chen, K. Amine, Ionic conductivity, lithium insertion and extraction of lanthanum lithium titatnate, Solid State Ionics 144 (2001) 51–57.
[39] M. Bengisu, Engineering Ceramics, Springer, 2001.
[40] R.A. Huggins, Use of defect equilibrium diagrams to understand minority species transport in solid electrolytes, Solid State Ionics 143 (2001) 3–16.
[41] J. Maier, M. Holzinger, W. Sitte, Fast potentiometric CO_2 sensors with open reference electrodes, Solid State Ionics 74 (1994) 5–9.
[42] M. Holzinger, J. Maier, A.W. Sitte, Fast CO_2-selective potentiometric sensor with open reference electrode, Solid State Ionics 86–88 (1996) 1055–1062.
[43] K.-Y. Yang, I.-C. Leu, K.-Z. Fung, M.-H. Hon, M.-C. Hsu, Y.-J. Hsiao, M.-C. Wang, Mechanism of the interfacial reaction between cation-deficient $La_{0.56}Li_{0.33}TiO_3$ and metallic lithium at room temperature, Journal of Materials Research 23 (2008) 1813–1825.
[44] Y. Harada, T. Ishigaki, H. Kawai, J. Kuwasno, Lithium ion conductivity of polycrystalline perovskite $La_{0.67-x}Li_{3x}TiO_3$ with ordered and disordered arrangements of the A-site ions, Solid State Ionics 108 (1998) 407–413.
[45] J.E. Bauerle, Study of solid electrolyte polarization by a complex admittance method, Journal of Physics and Chemistry of Solids 30 (1969) 2657–2670.
[46] J. Wolfenstine, J.L. Allen, J. Read, J. Sakamoto, G. Gonalez-Doncel, Hot-pressed $Li_{0.33}La_{0.57}TiO_3$, Journal of Power Sources 195 (2010) 4124–4128.
[47] C.W. Ban, G.M. Choi, The effect of sintering on the grain boundary conductivity of lithium lanthanum titanates, Solid State Ionics 140 (2001) 285–292.
[48] J.-S. Lee, K.S. Yoo, T.S. Kim, H.J. Jung, Evaluation of the AC response of Li-electrolytic perovskites $Li_{0.5}(Ln_xLa_{0.5-x})TiO_3$ (Ln = Nd, Gd) in conjunction with their crystallographic and microstructural chatacterisitcs, Solid State Ionics 98 (1997) 15–26.
[49] Hiroo Kawai, J. Kuwano, Lithium ion conductivity of A-site deficient Perovskite solid solution $La_{0.67-x}Li_{3x}TiO_3$, Journal of Electrochemical Society 141 (1994) L78–L79.
[50] A. Caroline, Kirk, A.R. West, Crystal structure of the perovskite-related phase of approximate composition $LaLi_{1/3}Ti_{2/3}O_3$, Solid State Sciences 4 (2002) 1163–1166.
[51] T. Albina, Borisevich, P.K. Davis, $La(Li_{1/3}Ti_{2/3})O_3$: a new 1:2 ordered perovskite, Journal of Solid State Chemistry 170 (2003) 198–201.
[52] J.-W. Kim, Y.-D. Lee, Y.-B. Kang, H.-G. Lee, Decomposition of Li_2CO_3 in existence of SiO_2 in mould flux of steel casting, in: VII International Conference on Molten Slags Fluxes and Salts, The South African Institute of Mining and Metallurgy, 2004.
[53] A. Boulant, J.F. Bardeau, A. Jouanneaux, J. Emery, J.-Y. Buzare, O. Bohnk, Reaction mechanisms of $Li_{0.30}La_{0.57}TiO_3$ powder with ambient air: H^+/Li^+ exchange with water and Li_2CO_3 formation, Dalton Transactions 39 (2010) 3968–3975.

Biographies

Junro Yoon received his B.S. in 2006 and M.S. in 2008 in Materials Science and Engineering from Hanyang University, Korea. This paper is based on his Ph.D. dissertation in the Department of Materials Science and Engineering of The Ohio State University.

Gary W. Hunter is the Lead for Intelligent System Hardware and the Technical Lead for the Chemical Species Gas Sensors Team in the Sensors and Electronics Branch at NASA Glenn Research Center. He has been involved with the design, fabrication, and testing of sensors for over 20 years. His work has included the use of micro and nano technology, the integration of sensor technology into smart systems, and the demonstration and application of sensor technology for a range of applications.

Sheikh Akbar is a Professor of Materials Science and Engineering and Founder of the NSF Center for Industrial Sensors and Measurements (CISM) at The Ohio State University. He obtained his Ph.D. from Purdue University in 1985. His current research deals with synthesis-microstructure-property relations of ceramic bulk, thin-film and nano-structures for electrochemical devices such as chemical sensors and fuel cells, and biomedical applications.

Prabir K. Dutta received his PhD degree in chemistry from Princeton University. After four years of industrial research at Exxon Research and Engineering Company, he joined The Ohio State University, where currently he is a Professor of Chemistry. His research interests are in the area of microporous materials, including their synthesis, structural analysis and as hosts for chemical and photochemical reactions.